Physica B 598 (2020) 412416

Contents lists available at ScienceDirect

Physica B: Physics of Condensed Matter

journal homepage: http://www.elsevier.com/locate/physb

A theoretical approach to the structural, elastic and electronic properties of $Ti_{8-x}V_{4-y}Mo_{x+y+z}Al_{4-z}$ lightweight shape memory alloys for biomaterial implant applications

C. Soykan

Vocational School of Health Services, Kırşehir Ahi Evran University, Kırşehir, Turkey

ARTICLE INFO

Keywords:
Lightweight shape memory alloys
$Ti_{8-x}V_{4-y}Mo_{x+y+z}Al_{4-z}$ alloy
Mechanical properties
Electronic structure
Ab-initio calculations

ABSTRACT

The physical properties of the off-stoichiometric $Ti_{8-x}V_{4-y}Mo_{x+y+z}Al_{4-z}$ alloys to reduce toxic effects and increase biomaterial efficiency have been studied systematically with Density Functional Theory (DFT) based ab-initio calculation methods. The calculated formation and cohesive energies show that thermodynamic and structural stability of the $Ti_{8-x}V_{4-y}Mo_{x+y+z}Al_{4-z}$ alloys increases due to the increase in Mo concentration. The results of Pugh's ratio (G/B) show that the ductility of all phases decreases with increasing Mo concentration (0.15 → 0.35). The plasticity of the $Ti_{8-x}V_{4-y}Mo_{x+y+z}Al_{4-z}$ alloys is downgraded with the increase of Mo concentration by the Poisson's ratio υ. The Young's modulus E of $Ti_8V_4Mo_3Al_1$ and $Ti_8V_3Mo_4Al_1$ phases were calculated as 49.84 GPa and 48.71 GPa, respectively. These phases are very suitable candidates for real biomaterial applications. Further, the electronic structure shows that as Mo concentration increases the Ti-3d-Mo-4d bonds become stronger and phases become more stable by the effect of Ti–Mo bonds.

1. Introduction

During the past few decades years, the alloys able to many efficient shape memory properties have been developed. Ti-based alloys have been used in many industries by using their superelastic behavior. However, there is a need to develop lightweight shape memory alloys (LWSMA) for areas such as aerospace, space, and biomaterials. The Ti–V–Al alloy, which is the subject of this article, is a very good candidate for LWSMAs with a density of approximately 4.5 g/cm^3. In addition to its low density, it is also very efficient in terms of cold workability (approximately 90% thickness) [1].

Ti-based alloys have recently been the most widely used shape memory alloys for implant applications because of their excellent biocompatibility, good mechanical properties, and high corrosion resistance [2,3]. However, Titanium, which is one of the elements that make up the Ti–V–Al alloy, is very slightly hazardous to health. Moreover, it has a high chemical exchange capacity and a high modulus of elasticity. Vanadium, on the other hand, is an element which is harmful to health and highly cytotoxic [4–7]. Aluminum is an element that is harmless in terms of health than others but can become unstable when heated and might induce senile dementia [4–7]. Besides, Molybdenum is a harmless, non-toxic, and non-allergic element compared to Ti, V, and Al in terms of health. It is a stable and β-stabilizing element. Moreover, Molybdenum has excellent biocompatibility for the human body [8]. Studies have shown that the substitution of Molybdenum in the range of approximately 15%–20% with Titanium can reduce the modulus of elasticity of Ti-based alloys. Thus, new Ti-based alloys with mechanical behaviors that can work more in harmony with the human body can be developed [8]. Ti–6Al–4V (TC4), which the widely used biomedical implant for bone-teeth and pure Titanium is the first Ti-based commercial alloys. Studies on these alloys have shown that element Vanadium produces harmful oxides in the human body, among other damages [9,10].

Recently, researchers have focused on the development of Ti–Mo-based alloys more suited to the human body with low elasticity modulus, high corrosion resistance, good surface characteristics, non-toxic, and non-allergenic. For this purpose, the studies focused on Ti–36Nb–2Ta–3Zr, Ti–24Nb–4Zr–7.8Sn, Ti–25Nb–3Mo–3Zr–2Sn, Ti–7Nb–10Mo, $Ti_{15-x}Mo_xSn$ [11–15], etc.

When the previous studies are examined, it is seen that by doping Mo element into Ti–V–Al alloys, toxic and allergic properties of the alloys and high modulus of elasticity can be reduced. In this way, it is clear that the compatibility of Ti-based alloys to the human body can be improved. For this purpose, the content of this study is based on a systematic

E-mail address: cengiz.soykan@ahievran.edu.tr.

https://doi.org/10.1016/j.physb.2020.412416
Received 13 February 2020; Received in revised form 7 July 2020; Accepted 30 July 2020
Available online 12 August 2020

examination of the structural, mechanical, and electronic properties of the off-stoichiometric $Ti_{8-x}V_{4-y}Mo_{x+y+z}Al_{4-z}$ alloy formed by the substitution of the element Mo instead of Titanium and Vanadium elements. Consciously, the concentration of Aluminum is fixed at a minimum of 6.25%. In this way, due to the Molybdenum substitution, while the toxic and allergic properties of the off-stoichiometric $Ti_{8-x}V_{4-y}Mo_{x+y+z}Al_{4-z}$ alloy are minimized, we will try to determine the optimal concentration for the human body in terms of mechanical behavior.

To the best of our knowledge, no theoretical studies on the structural, elastic and electronic properties of the off-stoichiometric $Ti_{8-x}V_{4-y}Mo_{x+y+z}Al_{4-z}$ alloys for our selected concentrations ($x = 0 \rightarrow 0 \leq y \leq 3, y = 0 \rightarrow 1 \leq x \leq 7$ and fixed at $z = 3$) by using the ab-*initio* calculation is available in the literature. Therefore, the results of our study will contribute to the literature in terms of developing new Ti–Mo based alloys for potential biomedical applications.

2. Computational method

In this study, ab-initio simulation calculations based on the Density Functional Theory (DFT) were performed using the potential of the projector augmented wave (PAW) to solve the Kohn-Sham equations [16–18]. Total energy calculations were performed using the Vienna ab-initio simulation package (VASP) [19–23]. The effects of electronic exchange and correlation functions were considered using the Generalized Gradient Approximation (GGA) developed by Burke, Perdew, and Ernzerhof [24]. In this study, the off-stoichiometric β-phase crystal form was generated in the $Ti_{8-x}V_{4-y}Mo_{x+y+z}Al_{4-z}$ format by using ($x = 0 \rightarrow 0 \leq y \leq 3, y = 0 \rightarrow 1 \leq x \leq 7$ and fixed at $z = 3$) values. In our calculations, the kinetic energy cutoff value for the $Ti_{8-x}V_{4-y}Mo_{x+y+z}Al_{4-z}$ crystal phase was determined to be 500 eV. The energy convergence criterion of the electronic self-consistency was chosen as 10^{-5} *eV/ atom* [25]. The Brillouin zone integrations were carried out by Monkhorst-Pack special points mesh with a grid size of 10 × 10 × 10 for $Ti_{8-x}V_{4-y}Mo_{x+y+z}Al_{4-z}$ crystal form [26]. The contribution of valence electrons is influential in determining the electronic properties of a material. In our study, the valence electron configurations for Ti, V, Al and Mo atoms are $3s^2 3p^6 4s^2 3d^2$, $3s^2 3p^6 4s^2 3d^3$, $2s^2 2p^6 3s^2 3p^1$ and $5s^2 4d^4$, respectively.

Goldschmidt's rules should be considered to examine the process of the placement of Mo atom instead of Ti and V atoms by using ($x = 0 \rightarrow 0 \leq y \leq 3$, $y = 0 \rightarrow 1 \leq x \leq 7$ and fixed at $z = 3$) values in $Ti_{8-x}V_{4-y}Mo_{x+y+z}Al_{4-z}$ lightweight shape memory alloys. The empirical rules for element substitution for Goldschmidt, if the ionic radius differs by less than 15%, a full perfectly substitution can occur, but, if the size differs between 15 and 30%, limited substitution can occur. Thus, the charge of the material changes, and the charge neutrality is restored by changing the charges of the other elements [27]. The difference between the ionic radius of Mo ($Mo^{3+} = 83$ pm) and the ionic radii of Ti ($Ti^{3+} = 81$ pm) and V ($V^{3+} = 78$ pm) were calculated to be 2.47% and 6.41%, respectively. Since this difference between the ionic radii is less than 15%, it can be said that a full perfectly substitution can be achieved in terms of Goldschmidt's empirical substitution rules. In this study, to determine the electronic behavior of the material, the density of electronic states (DOS) and the partial electronic density of states (pDOS) were calculated using the tetrahedron method involving the Bloch corrections. In the DOS calculations, the k-mesh numbers are increased to 20 × 20 × 20 for all crystal models.

$Ti_{8-x}V_{4-y}Mo_{x+y+z}Al_{4-z}$ alloys with β-type 16 atoms were formed in the form of 2 × 2 × 2 supercells. The distribution of Mo atoms into the 2 × 2 × 2 supercell was carried out using the special quasi-random structures (SQS) method [28,29]. Al concentration was selected to be 6.25%. Off-stoichiometric $Ti_8V_4Mo_3Al_1$, $Ti_8V_3Mo_4Al_1$, $Ti_8V_2Mo_5Al_1$, $Ti_8V_1Mo_6Al_1$, $Ti_7V_1Mo_7Al_1$, $Ti_6V_1Mo_8Al_1$, $Ti_5V_1Mo_9Al_1$, $Ti_4V_1Mo_{10}Al_1$, $Ti_3V_1Mo_{11}Al_1$, $Ti_2V_1Mo_{12}Al_1$ and $Ti_1V_1Mo_{13}Al_1$ alloys were formed as a result of the substitution of the Mo atoms in the appropriate Ti and V atoms positions. Mo concentrations corresponding to these off-stoichiometric crystal forms are 18.75, 25.00, 31.25, 37.50, 43.75, 50.00, 56.25, 62.50, 68.75, 75.00 and 81.25 at % Mo in the alloy, respectively. The calculated off-stoichiometric crystal forms are shown in Fig. 1.

3. Results and discussion

3.1. Off-stoichiometric crystal structural properties

The ground state equilibrium lattice parameters of the compounds given in Table 1 were calculated at 0 K and 0 GPa. According to our results, $Ti_8V_4Mo_3Al_1$, $Ti_8V_3Mo_4Al_1$ and $Ti_8V_1Mo_6Al_1$ crystal compounds retain their cubic character while other compounds have undergone phase transition to tetragonal, rhombohedral and monoclinic. In the study by Otsuka and Ren about the phase transitions of Ti-based shape memory alloys, it has been reported that the tetragonal crystal structures were observed at high temperatures while the orthorhombic structures were seen at low temperatures of these alloys [30,31]. In addition, it has been stated that phase transitions of Ti-based alloys can be realized from cubic to monoclinic martensite [30]. On the other hand, the presence of a rhombohedral crystal structure has been shown in Ref. [32,33] for Ti-based alloys. Finally, The lattice constants of this structure were calculated by Saburi, Tadaki et al. [33,34]. The simulation results summarized in Table 1 shows that the lattice parameters of the rhombohedral phases are equal, the angles are quite close to 90°. As such, the rhombohedral phases show a very close character to the cubic phase.

As is well known to all, for a compound to be in thermodynamic stability, its formation energy must be negative. Also, the formation of compound form becomes easier as long as the formation of energy has a more negative value. In addition to the formation of energy, the value of cohesive energy is very important for thermodynamic stability. The lower the cohesive energy of the phase, the more stable the phase will be. To see and compare the stability of 11 number off-stoichiometric phases in $Ti_{8-x}V_{4-y}Mo_{x+y+z}Al_{4-z}$ form, the formation and cohesive energy of each phase were calculated. In the calculation of the formation energy, the function given below is used [35].

$$E_{for} = \frac{1}{(n_{Ti} + n_V + n_{Mo} + n_{Al})}\left[E_{total} - \left(n_{Ti}E^{Ti}_{solid} + n_V E^{V}_{solid} + n_{Mo}E^{Mo}_{solid} + n_{Al}E^{Al}_{solid}\right)\right] \quad (1)$$

where, E_{tot} is the unit cell total energy in the equilibrium state of the studied phases. Also, E^{Ti}_{solid}, E^{V}_{solid}, E^{Mo}_{solid} and E^{Al}_{solid} are the ground state energy of Ti, V, Mo, and Al atoms, respectively. Also, n_{Ti}, n_V, n_{Mo} and n_{Al} represent the number of Ti, V, Mo, and Al atoms in the unit cell.

The function used in the calculation of cohesive energy is as follows [36]:

$$E_{coh} = \frac{1}{(n_{Ti} + n_V + n_{Mo} + n_{Al})}\left[\left(E_{total} - n_{Ti}E^{Ti}_{atom} + n_V E^{V}_{atom} + n_{Mo}E^{Mo}_{atom} + n_{Al}E^{Al}_{atom}\right)\right] \quad (2)$$

Similarly, E^{Ti}_{atom}, E^{V}_{atom}, E^{Mo}_{atom} and E^{Al}_{atom} are the isolated state energy of Ti, V, Mo, and Al atoms, respectively. n_{Ti}, n_V, n_{Mo} and n_{Al} refer to the number of Ti, V, Mo, and Al atoms in the unit cell.

The calculated E_{for}, E_{coh} and the volume of unit cell V_0 for the off-stoichiometric $Ti_{8-x}V_{4-y}Mo_{x+y+z}Al_{4-z}$ compounds are given in Table 2. Our results show that the calculated formation energy for all phases is negative. The obtained negative formation energy values indicate that the great probability to form of all phases studied is high.

Besides, as shown in Fig. 2, the formation energy gets more negative as the Mo concentration more and more. Therefore, the thermodynamic stability of the $Ti_{8-x}V_{4-y}Mo_{x+y+z}Al_{4-z}$ compound is increased. Focusing on Fig. 2 shows that the cohesive energy decreases with increasing Mo concentration. Furthermore, the value of cohesive energy for all phases is negative. According to this result, increased Mo concentration makes

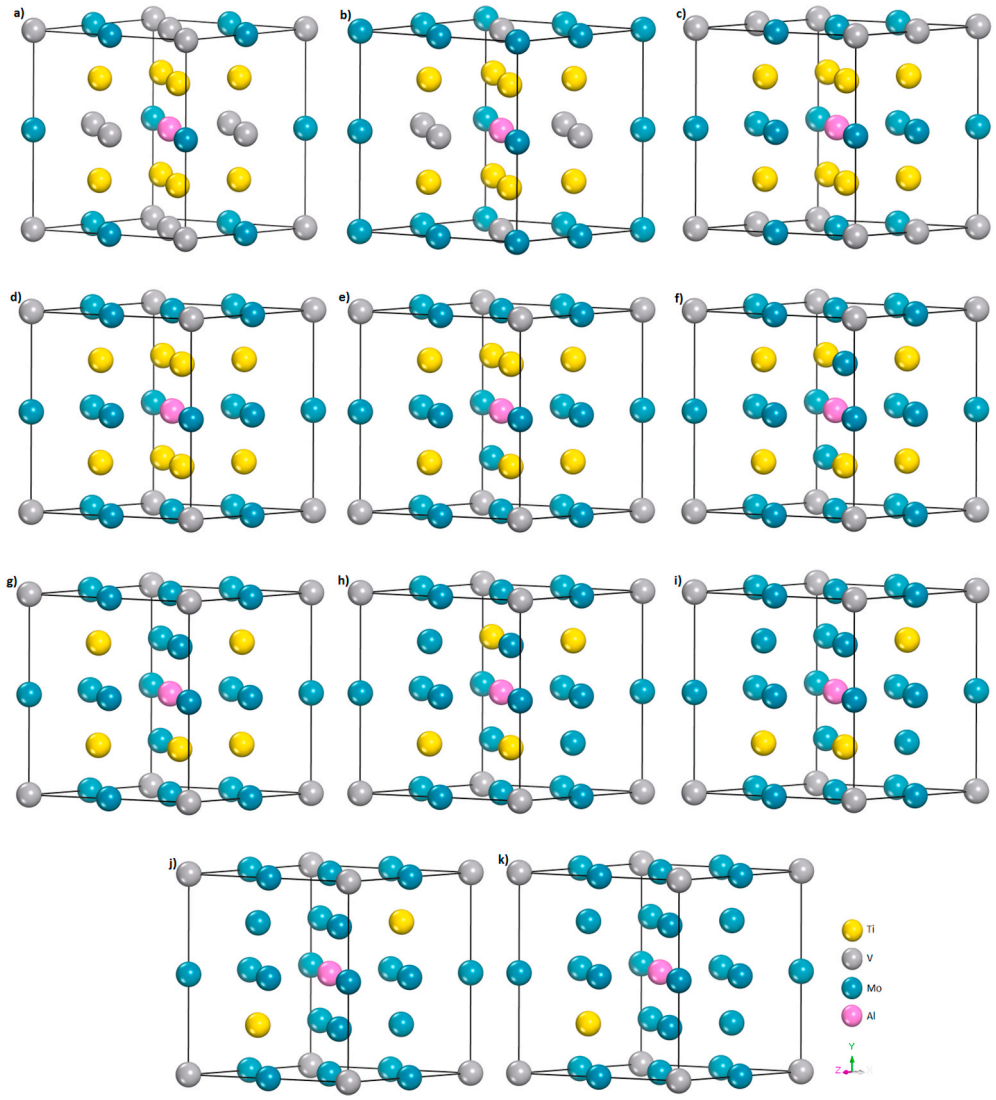

Fig. 1. The off-stoichiometric crystal structures models of $Ti_8V_4Mo_3Al_1$ (a), $Ti_8V_3Mo_4Al_1$ (b), $Ti_8V_2Mo_5Al_1$ (c), $Ti_8V_1Mo_6Al_1$ (d), $Ti_7V_1Mo_7Al_1$ (e), $Ti_6V_1Mo_8Al_1$ (f), $Ti_5V_1Mo_9Al_1$ (g), $Ti_4V_1Mo_{10}Al_1$ (h), $Ti_3V_1Mo_{11}Al_1$ (i), $Ti_2V_1Mo_{12}Al_1$ (j) and $Ti_1V_1Mo_{13}Al_1$ (k) compounds.

Table 1
The calculated lattice parameters of $Ti_{8-x}V_{4-y}Mo_{x+y+z}Al_{4-z}$ shape memory alloys by geometric optimization.

Compounds	a_0(Å)	b_0(Å)	c_0(Å)	α	β	γ	Phases
$Ti_8V_4Mo_3Al_1$	6.33773	6.33773	6.33773	90.0000	90.0000	90.0000	Cubic
$Ti_8V_3Mo_4Al_1$	6.34886	6.34886	6.34886	90.0000	90.0000	90.0000	Cubic
$Ti_8V_2Mo_5Al_1$	6.30188	6.30188	6.32078	90.0000	90.0000	90.0000	Tetragonal
$Ti_8V_1Mo_6Al_1$	6.31950	6.31950	6.31950	90.0000	90.0000	90.0000	Cubic
$Ti_7V_1Mo_7Al_1$	6.31497	6.31497	6.31497	89.8855	89.8855	89.8855	Rhombohedral
$Ti_6V_1Mo_8Al_1$	6.30542	6.30542	6.30542	89.8855	89.8855	89.8855	Rhombohedral
$Ti_5V_1Mo_9Al_1$	6.29222	6.29222	6.29026	89.8785	89.8785	89.9999	Monoclinic[a]
$Ti_4V_1Mo_{10}Al_1$	6.28192	6.28192	10.97579	125.9063	125.9063	88.5865	Monoclinic[a]
$Ti_3V_1Mo_{11}Al_1$	6.28293	6.28293	11.01010	125.6982	125.6982	89.2618	Monoclinic[a]
$Ti_2V_1Mo_{12}Al_1$	6.28387	6.28387	6.28387	89.4382	89.4382	89.4382	Rhombohedral
$Ti_1V_1Mo_{13}Al_1$	6.28113	6.28113	6.28113	89.8570	89.8570	89.8570	Rhombohedral

[a] The lattice type of star-marked structures are primitive of the C-centered monoclinic.

the crystal system more stable. However, our calculations showed that the increased Mo concentration makes the phases more stable, but also leads to phase transitions.

3.2. *Off-stoichiometric crystal elastic and mechanical properties*

It is a good way to use elastic constants to obtain information about the mechanical behavior of materials. In particular, whether a crystal form is mechanically stable can be determined by calculating its elastic constants. Mathematically necessary and sufficient stability conditions

Table 2
The calculated cohesive energy E_{coh}, formation energy E_{for} and unit cell volume V_0 for $Ti_{8-x}V_{4-y}Mo_{x+y+z}Al_{4-z}$ shape memory alloys.

Compounds	E_{coh}(kJ/mol)per atom	E_{for}(kJ/mol)per atom	V_0(Å^3)
$Ti_8V_4Mo_3Al_1$	−702.16344	−20.97312	253.80
$Ti_8V_3Mo_4Al_1$	−718.83013	−24.01409	255.14
$Ti_8V_2Mo_5Al_1$	−735.12681	−26.68506	250.26
$Ti_8V_1Mo_6Al_1$	−751.58814	−29.52067	251.62
$Ti_7V_1Mo_7Al_1$	−776.08263	−32.53578	251.06
$Ti_6V_1Mo_8Al_1$	−800.11535	−35.08912	249.94
$Ti_5V_1Mo_9Al_1$	−823.97691	−37.47129	248.99
$Ti_4V_1Mo_{10}Al_1$	−847.43994	−39.45495	248.24
$Ti_3V_1Mo_{11}Al_1$	−870.41757	−40.95320	248.03
$Ti_2V_1Mo_{12}Al_1$	−892.57751	−41.63376	247.35
$Ti_1V_1Mo_{13}Al_1$	−914.26434	−41.84121	247.06

for a crystal system to be mechanically stable can be listed as follows [37]:

- The matrix Cij is definite positive;
- All eigenvalues of Cij are positive;
- Sylvester's criterion must be provided;
- An arbitrary set of minors of C are all positive.

The four possible formulations are called the Born elastic stability conditions for an unstressed crystal system. They are valid regardless of the symmetry of the crystal and are not linear [37].

To determine the mechanical behavior of the non-stoichiometric $Ti_{8-x}V_{4-y}Mo_{x+y+z}Al_{4-z}$ alloys, theoretically elastic constants were calculated using the appropriate VASP flags. The elastic constants of $Ti_{8-x}V_{4-y}Mo_{x+y+z}Al_{4-z}$ material were calculated by the linear response method. Some flags in the VASP code allows determining the Hessian matrix and the only zone centered Γ- point vibrational frequencies of a crystal phase. The Hessian matrix can be estimated from the second derivative of total energy using the finite differences method and the positions of all atoms. Finally, the elastic tensor can be calculated using the six-finite deformation of the crystal lattice. During this calculation, rigid and movable ions and the strain-stress relationship of elastic constants are used [38]. The calculated elastic stiffness constants for all phases of $Ti_{8-x}V_{4-y}Mo_{x+y+z}Al_{4-z}$ alloys are listed in Table 3.

In this study, the Voigt-Reuss-Hill approximations were applied to the calculation of the bulk modulus B, shear modulus G and Young's modulus E for the off-stoichiometric $Ti_{8-x}V_{4-y}Mo_{x+y+z}Al_{4-z}$ crystal structures. For all phases by crystal symmetry, the Voigt bulk modulus B_V, Reuss bulk modulus B_R, Voigt shear modulus G_V, Reuss shear modulus G_R, Voigt-Reuss-Hill bulk modulus B, shear modulus G, Young's modulus E, and mechanical stability criteria are given below, respectively. For all phases, the bulk modulus B and shear modulus G can be obtained by calculating Voigt and Reuss bounds and averaging

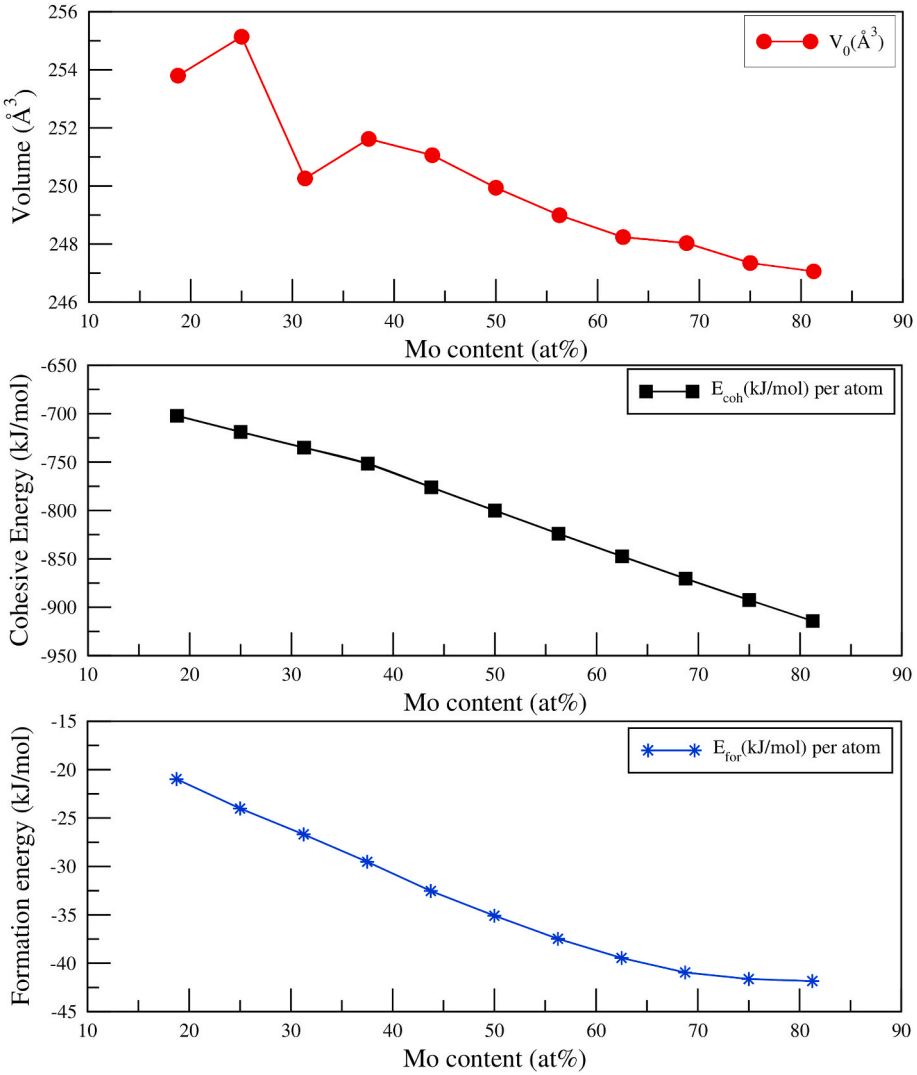

Fig. 2. The calculated unit cell volume V_0, cohesive energy E_{coh} and formation of energy E_{for} for $Ti_{8-x}V_{4-y}Mo_{x+y+z}Al_{4-z}$ shape memory alloys.

Table 3
The calculated elastic constants $C_{ij}(GPa)$ for $Ti_{8-x}V_{4-y}Mo_{x+y+z}Al_{4-z}$ shape memory alloys.

Compounds	$C_{11}(GPa)$	$C_{12}(GPa)$	$C_{13}(GPa)$	$C_{22}(GPa)$	$C_{33}(GPa)$	$C_{44}(GPa)$	$C_{55}(GPa)$	$C_{66}(GPa)$
$Ti_8V_4Mo_3Al_1$	123.92	112.35				34.98		
$Ti_8V_3Mo_4Al_1$	151.01	120.04				17.98		
$Ti_8V_2Mo_5Al_1$	333.57	132.30	151.42		286.63	45.87		44.88
$Ti_8V_1Mo_6Al_1$	200.28	117.11				40.11		
$Ti_7V_1Mo_7Al_1$	218.70	136.92	141.84		200.33	47.93		40.89
$Ti_6V_1Mo_8Al_1$	203.66	142.08	150.37		184.30	39.62		30.79
$Ti_5V_1Mo_9Al_1$	299.87	272.03	130.73	314.10	318.73	35.97	13.54	136.84
$Ti_4V_1Mo_{10}Al_1$	490.73	366.52	174.41	457.68	353.85	50.23	31.48	224.44
$Ti_3V_1Mo_{11}Al_1$	310.85	170.76	182.48	396.63	297.95	153.61	116.17	104.04
$Ti_2V_1Mo_{12}Al_1$	428.66	222.49	245.67		382.00	97.75		103.09
$Ti_1V_1Mo_{13}Al_1$	403.47	207.58	227.11		404.20	108.61		97.94

term ($B = (B_V + B_R)/2, G = (G_V + G_R)/2$).

The mechanical criteria for cubic crystals at 0 GPa are given following [39–45]:

$$(C_{11} - C_{12}) > 0, C_{11} > 0, C_{44} > 0, C_{11} + 2C_{12} > 0, C_{12} < B < C_{11} \tag{3}$$

Voigt-Reuss-Hill bulk modulus B and shear modulus G are given as follows:

$$B = B_V = B_R = \frac{(C_{11} + 2C_{12})}{3} \tag{4}$$

$$G = \frac{G_V + G_R}{2} = \frac{1}{2}\left[\frac{1}{5}(3C_{44} + C_{11} - C_{12}) + \frac{5(C_{11} - C_{12})C_{44}}{4C_{44} + 3(C_{11} - C_{12})}\right] \tag{5}$$

For tetragonal crystals these mechanical stability restrictions are as follows [40]:

$$\begin{aligned} &(C_{11} - C_{12}) > 0, C_{11} > 0, C_{33} > 0, C_{44} > 0, C_{66} > 0, \\ &(C_{11} + C_{33} - 2C_{13}) > 0, (2C_{11} + C_{33} + 2C_{12} + 4C_{13}) > 0, \\ &\frac{1}{3}(C_{12} + 2C_{13}) < B < \frac{1}{3}(C_{11} + 2C_{33}). \end{aligned} \tag{6}$$

In the tetragonal phases, Voigt-Reuss-Hill bulk modulus B and shear modulus G are given as follows [46–48]:

$$B = \frac{B_V + B_R}{2} = \frac{1}{2}\left[\frac{1}{9}(2(C_{11} + C_{12}) + C_{33} + 4C_{13}) + \frac{(C_{11} + C_{12})C_{33} - 2C_{13}^2}{C_{11} + C_{12} + 2C_{33} - 4C_{13}}\right] \tag{7}$$

$$G = \frac{G_V + G_R}{2} = \frac{1}{2}\left[\frac{1}{30}(4C_{11} - 2C_{12} + 2C_{33} - 4C_{13} + 12C_{44} + 6C_{66}) + \left(\frac{15}{18\left(\frac{1}{9}(2C_{11} + 2C_{12} + C_{33} + 4C_{13})\right)}{\left((C_{11} + C_{12})C_{33} - 2C_{13}^2\right)} + \frac{6}{(C_{11} - C_{12})} + \frac{6}{C_{44}} + \frac{3}{C_{66}}\right)\right] \tag{8}$$

The mechanical stability criteria of the rhombohedral phase are given as follows [39]:

$$\begin{aligned} &(C_{11} + C_{12}) > 0, C_{33} > 0, (C_{11} + C_{12})C_{33} > 2C_{13}^2 \\ &(C_{11} - C_{12}) > 0, C_{44} > 0, (C_{11} - C_{12})C_{44} > 2C_{14}^2 \end{aligned} \tag{9}$$

Voigt-Reuss-Hill bulk modulus B and shear modulus G in the rhombohedral phase are given as follows by using the elastic stiffness constants (C_{ij}) and elastic compliance constants (S_{ij}) [49]:

$$B = \frac{B_V + B_R}{2} = \frac{1}{2}\left[\frac{1}{9}(2C_{11} + 2C_{12} + 4C_{13} + C_{33}) + \frac{1}{2S_{11} + 2S_{12} + 4S_{13} + S_{33}}\right] \tag{10}$$

$$G = \frac{G_V + G_R}{2} = \frac{1}{2}\left[\frac{1}{30}(7C_{11} - 5C_{12} - 4C_{13} + 2C_{33} + 12C_{44}) + \left(\frac{15}{14S_{11} - 10S_{12} - 8S_{13} + 4S_{33} + 6S_{44}}\right)\right] \tag{11}$$

The C_{14} elastic stiffness constants of $Ti_7V_1Mo_7Al_1$, $Ti_6V_1Mo_8Al_1$, $Ti_2V_1Mo_{12}Al_1$ and $Ti_1V_1Mo_{13}Al_1$ rhombohedral structures are 3.23 GPa, 4.31 GPa, 43.95 GPa, and 23.94 GPa, respectively. Further, the elastic compliance constants S_{11}, S_{12}, S_{13}, S_{33}, and S_{44} are 0.009378 GPa^{-1}, -0.0029161 GPa^{-1}, -0.004575 GPa^{-1}, 0.011470 GPa^{-1}, and 0.020974 GPa^{-1} for $Ti_7V_1Mo_7Al_1$. The elastic compliance constants S_{11}, S_{12}, S_{13}, S_{33}, and S_{44} are 0.013228 GPa^{-1}, -0.003263 GPa^{-1}, -0.008130 GPa^{-1}, 0.018694 GPa^{-1}, and 0.025630 GPa^{-1} for $Ti_6V_1Mo_8Al_1$. The elastic compliance constants S_{11}, S_{12}, S_{13}, S_{33}, and S_{44} are 0.004491 GPa^{-1}, -0.001508 GPa^{-1}, -0.001918 GPa^{-1}, 0.005085 GPa^{-1}, and 0.012655 GPa^{-1} for $Ti_2V_1Mo_{12}Al_1$, The elastic compliance constants S_{11}, S_{12}, S_{13}, S_{33}, and S_{44} are 0.004103 GPa^{-1}, -0.001292 GPa^{-1}, -0.001579 GPa^{-1}, 0.004248 GPa^{-1}, and 0.009731 GPa^{-1} for $Ti_1V_1Mo_{13}Al_1$.

The C_{23}, C_{35}, C_{46}, C_{25} and C_{15} elastic constants of $Ti_5V_1Mo_9Al_1$ the C-centered monoclinic are 150.79 GPa, 6.62 GPa, 3.08 GPa, 1.79 GPa and 5.94 GPa, respectively. The C_{23} of $Ti_4V_1Mo_{10}Al_1$ the C-centered monoclinic is 184.16 GPa and the other elastic constants are zero. Finally, The C_{23}, C_{35}, C_{46}, C_{25} and C_{15} elastic constants of $Ti_3V_1Mo_{11}Al_1$ the C-centered monoclinic are 239.58 GPa, 49.70 GPa, 69.95 GPa, 88.49 GPa, and 6.53 GPa, respectively. These constants are not listed in Table 3.

Finally, for a monoclinic structure, the more complicated criteria are expected. These mechanical stability criteria are given by Watt et al. as follows [50]:

$$\begin{aligned}&\left(C_{23}C_{33}-{C_{23}}^2\right)>0,\left(C_{33}C_{55}-{C_{35}}^2\right)>0,\left(C_{44}C_{66}-{C_{46}}^2\right)>0C_{11}+C_{22}C_{33}+2(C_{12}+C_{13}+C_{23})>0C_{22}\left(C_{33}C_{55}-{C_{35}}^2\right)+2\left(C_{23}C_{25}C_{35}-{C_{25}}^2(C_{55}-C_{33})\right)>02\\&\left[C_{15}C_{25}(C_{33}C_{12}-C_{13}C_{23})+C_{15}C_{35}(C_{22}C_{13}-C_{12}C_{23})+C_{25}C_{35}(C_{11}C_{23}-C_{12}C_{13})-{C_{15}}^2\left(C_{22}C_{33}-{C_{23}}^2\right)+{C_{25}}^2\left(C_{11}C_{33}-{C_{13}}^2\right)+{C_{35}}^2\left(C_{11}C_{22}-{C_{12}}^2\right)\right]\\&+C_{55}\left(C_{11}C_{22}C_{33}-C_{11}{C_{23}}^2-C_{22}{C_{13}}^2-C_{33}{C_{12}}^2+2C_{12}C_{13}C_{23}\right)>0\end{aligned}\tag{12}$$

The homogenized elastic properties of monoclinic phase can be calculated, of which bulk modulus can be obtained by calculating Voigt and Reuss bounds and averaging term as [51]:

$$B_V=\frac{1}{9}\left[C_{11}+C_{22}+C_{33}+2(C_{12}+C_{13}+C_{23})\right]\tag{13}$$

$$\begin{aligned}\Omega=2&\left[C_{15}C_{25}(C_{33}C_{12}-C_{13}C_{23})+C_{15}C_{35}(C_{22}C_{13}-C_{12}C_{23})+C_{25}C_{35}(C_{11}C_{23}\right.\\&\left.-C_{12}C_{13})\right]-\left[{C_{15}}^2\left(C_{22}C_{33}-{C_{23}}^2\right)+{C_{25}}^2\left(C_{11}C_{33}-{C_{13}}^2\right)+{C_{35}}^2\left(C_{11}C_{22}\right.\right.\\&\left.\left.-{C_{12}}^2\right)\right]+gC_{55}\end{aligned}\tag{14}$$

$$g=C_{11}C_{22}C_{33}-C_{11}{C_{23}}^2-C_{22}{C_{13}}^2-C_{33}{C_{12}}^2+2C_{12}C_{13}C_{23}\tag{15}$$

$$\begin{aligned}f=&C_{11}\left(C_{22}C_{55}-{C_{25}}^2\right)-C_{12}(C_{12}C_{55}-C_{15}C_{25})+C_{15}(C_{12}C_{25}-C_{15}C_{22})\\&+C_{25}(C_{23}C_{35}-C_{25}C_{33})\end{aligned}\tag{16}$$

Reuss bulk modulus can be calculated using equations (14)–(16) as follows:

$$\begin{aligned}B_R=\Omega&\left[\left(C_{33}C_{55}-{C_{35}}^2\right)(C_{11}+C_{22}-2C_{12})+(C_{23}C_{55}-C_{25}C_{35})\right.\\&(2C_{12}-2C_{11}-C_{23})+(C_{13}C_{35}-C_{15}C_{33})(C_{15}-2C_{25})+(C_{13}C_{55}\\&-C_{15}C_{35})(2C_{12}+2C_{23}-C_{13}-2C_{22})+2(C_{13}C_{25}\\&\left.-C_{15}C_{23})(C_{25}-C_{15})+f\right]^{-1}\end{aligned}\tag{17}$$

Similarly, Voigt-Reuss shear modulus can be calculated using equations (14)–(16) as follows:

$$G_V=\frac{1}{15}\left[C_{11}+C_{22}+C_{33}+3(C_{44}+C_{55}+C_{66})-(C_{12}+C_{13}+C_{23})\right]\tag{18}$$

$$\begin{aligned}G_R=15&\left[4\left[\left(C_{33}C_{55}-C_{35}^2\right)(C_{11}+C_{22}+C_{12})+(C_{23}C_{55}-C_{25}C_{35})\right.\right.\\&(C_{11}-C_{12}-C_{23})+(C_{13}C_{35}-C_{15}C_{33})(C_{15}+C_{25})+(C_{13}C_{55}\\&-C_{15}C_{35})(C_{22}-C_{12}-C_{23}-C_{13})+(C_{13}C_{25}\\&\left.\left.-C_{15}C_{23})(C_{15}-C_{25})+f\right]\Big/\Omega+3\left[\frac{g}{\Omega}+\frac{(C_{44}+C_{66})}{(C_{44}C_{66}-C_{46}^2)}\right]\right]^{-1}\end{aligned}\tag{19}$$

The bulk modulus B and shear modulus G of the monoclinic structure was calculated by averaging equations (13)–(19), respectively. The calculated bulk modulus B and shear modulus G data of all phases are presented in Table 4.

It is seen that all the calculated elastic constants of the off-stoichiometric $Ti_{8-x}V_{4-y}Mo_{x+y+z}Al_{4-z}$ structure meet all the mechanical stability conditions given above according to the crystal symmetries. This result shows that all phases are mechanically stable at zero pressure. Elastic constants C_{11}, C_{12} and C_{44} are common constants that take value in all phases. Therefore, to examine the effect of increasing Mo concentration on elastic constants, as given in Fig. 3, the variation of these elastic constants was studied. Fig. 3 shows that the value of the elastic constant C_{11} increases monotonously for all phases due to the increase in Mo concentration. However, the value of the C_{11} elastic constant of the tetragonal $Ti_8V_2Mo_5Al_1$ and C-centered monoclinic $Ti_4V_1Mo_{10}Al_1$ phases abnormally increases. The value of C_{12} also increases with increasing Mo concentration. However, the amount of increase is slower than C_{11}. The monotone increase abnormally deteriorates in the $Ti_5V_1Mo_9Al_1$ and $Ti_4V_1Mo_{10}Al_1$ C-centered monoclinic phases, and the C_{12} elastic constant values of these phases suddenly increase. The C_{44} value of all phases increases uniformly with increasing Mo concentration. Only the amount of increase from the $Ti_3V_1Mo_{11}Al_1$ phase has an abnormal value. Due to the increase in Mo concentration, abnormal increases in elastic constants C_{11}, C_{12} and C_{44} are generally observed in tetragonal and monoclinic phases. As the Mo concentration increases in the cubic and rhombohedral phases, the values of the elastic constants increase monotonously. As shown in Fig. 2, the increased Mo concentration decreases both formation and cohesive energy, making the crystal system more stable. Due to the high symmetry of cubic structures, the values of elastic constants increase due to Mo increase. Furthermore, as given in Table 1, the mesh constants of the rhombohedral structures are equal, but the unit cell angles are different from 90°. However, the unit cell angles are very close to 90° (89.8855 ≅ 90.00). Then, it is a good approach to expect rhombohedral structures to exhibit similar behaviors to cubic structures. This expected behavior is seen in Fig. 3.

Young's modulus E and Poisson's ratio υ are very important

Table 4
The calculated bulk modulus B (GPa), shear modulus G(GPa), Young's modulus E(GPa), micro-hardness H(GPa), Pugh's ratio (G/B) and Poisson's ratio ν for $Ti_{8-x}V_{4-y}Mo_{x+y+z}Al_{4-z}$ shape memory alloys.

Compounds	B(GPa)	G(GPa)	E(GPa)	H(GPa)	G/B	ν
$Ti_8V_4Mo_3Al_1$	116.21	17.44	49.84	0.83	0.15	0.43
$Ti_8V_3Mo_4Al_1$	130.36	16.94	48.71	0.70	0.13	0.44
$Ti_8V_2Mo_5Al_1$	202.47	58.83	160.90	5.19	0.29	0.37
$Ti_8V_1Mo_6Al_1$	144.83	40.69	111.62	3.48	0.28	0.37
$Ti_7V_1Mo_7Al_1$	164.22	41.25	114.19	3.19	0.25	0.38
$Ti_6V_1Mo_8Al_1$	164.02	30.63	86.50	1.79	0.19	0.41
$Ti_5V_1Mo_9Al_1$	221.74	44.57	125.30	2.80	0.20	0.41
$Ti_4V_1Mo_{10}Al_1$	293.18	80.05	220.12	6.68	0.27	0.37
$Ti_3V_1Mo_{11}Al_1$	232.97	87.35	232.95	9.71	0.37	0.33
$Ti_2V_1Mo_{12}Al_1$	296.19	86.93	237.56	7.75	0.29	0.37
$Ti_1V_1Mo_{13}Al_1$	281.55	97.18	261.46	10.03	0.35	0.35

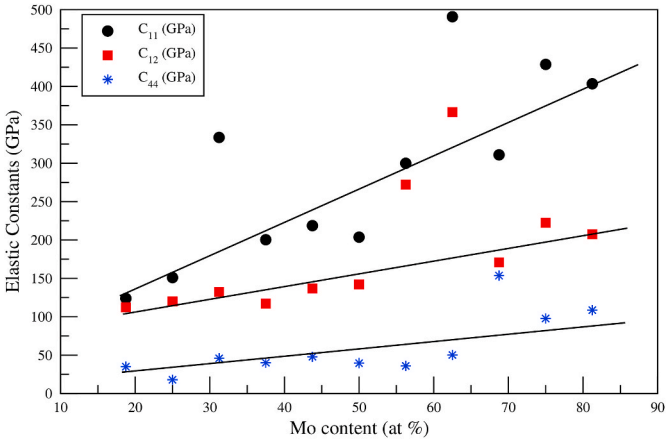

Fig. 3. The calculated elastic constants C_{ij}(GPa) for $Ti_{8-x}V_{4-y}Mo_{x+y+z}Al_{4-z}$ shape memory alloys and their shifting according to Mo content.

parameters in applications. It is noticeable that the human bone's Young's modulus is determined from 20 GPa to 40 GPa range and the materials are stiffer as young's modulus increase [52].

Young's modulus was computed by using the formula [53]:

$$E = \frac{9BG}{(3B + G)} \tag{20}$$

Young's modulus E can be considered as an indicator of the stiffness of solids. As Young's modulus E value increases, the stiffness of the materials increases. Further, by studying Young's modulus, an idea of whether a material can become used as biomaterial can be obtained. Young's modulus E of $Ti_8V_4Mo_3Al_1$ and $Ti_8V_3Mo_4Al_1$ phases were calculated as 49.84 GPa and 48.71 GPa, respectively. The human bone's Young's modulus E is in the range of 20–40 GPa. When our results are evaluated in terms of this criterion, $Ti_8V_4Mo_3Al_1$ and $Ti_8V_3Mo_4Al_1$ phases are very suitable candidates for real biomaterial applications. Also, with Young's modulus E of 86.5 GPa, the $Ti_6V_1Mo_8Al_1$ phase can be considered a good biomaterial candidate. Young's modulus E of all other phases except these phases is higher than 100 GPa. Therefore, these phases are structures with a very hard character nature.

The Poisson's ratio υ provides basic information about the nature of the chemical bonding forces of materials and their response to shear stress. The Poisson's ratio υ is calculated below given formula:

$$\upsilon = \frac{(3B - 2G)}{2(3B + G)} \tag{21}$$

The plasticity behavior of materials can be evaluated by focusing Poisson's ratio υ. The higher the Poisson ratio of the materials, the better the plasticity behavior. For covalent bonding force the Poisson's ratio is small ($\upsilon = 0.1$), and for ionic materials $\upsilon = 0.25$ or higher values [54]. As given in Table 4, the Poisson's ratio υ of all studied phases of the $Ti_{8-x}V_{4-y}Mo_{x+y+z}Al_{4-z}$ alloy is between 0.33 and 0.44. These calculated Poisson's ratio υ values indicate that the $Ti_{8-x}V_{4-y}Mo_{x+y+z}Al_{4-z}$ alloys have an ionic nature. Moreover, increasing Mo concentration reduces the Poisson's ratio. This behavior enhances the ionic character of the material and, as mentioned previously, increases the stability of the crystal structure. This result shows that using ionic radii of Ti^{3+}, V^{3+} and Mo^{3+} atoms are the correct approach in our study. Further, the plasticity of the $Ti_{8-x}V_{4-y}Mo_{x+y+z}Al_{4-z}$ alloys is decreased with the increase of Mo content.

Pugh's ratio is defined as G/B, which is a simple indicator of the correlation between the brittle-ductile characteristic of crystals and their elastic stiffness constants [55]. Brittle materials have a ratio of $G/B > 0.5$, while ductile is less than 0.5 value [56]. Young's modulus E, Poisson's ratio υ, and Pugh's ratio G/B for all phases studied in the $Ti_{8-x}V_{4-y}Mo_{x+y+z}Al_{4-z}$ alloys are given in Table 4. The calculated Pugh's ratio for all phases is between 0.15 and 0.37. Therefore, we studied all phases of material that have a ductile character. The highest ductility is in the $Ti_8V_3Mo_4Al_1$ phase while the lowest ductility in the $Ti_3V_1Mo_{11}Al_1$ phase. Also, although all phases remained within the limits of ductility, it was found that the Pugh's ratio increased due to the increased Mo concentration. In this respect, the substitution of Mo contributes to reducing the ductility of the material. Ductility ability is very important for biomaterials. The material must have a ductile nature to be able to withstand the applied force. In this respect, the results of our studies are satisfactory.

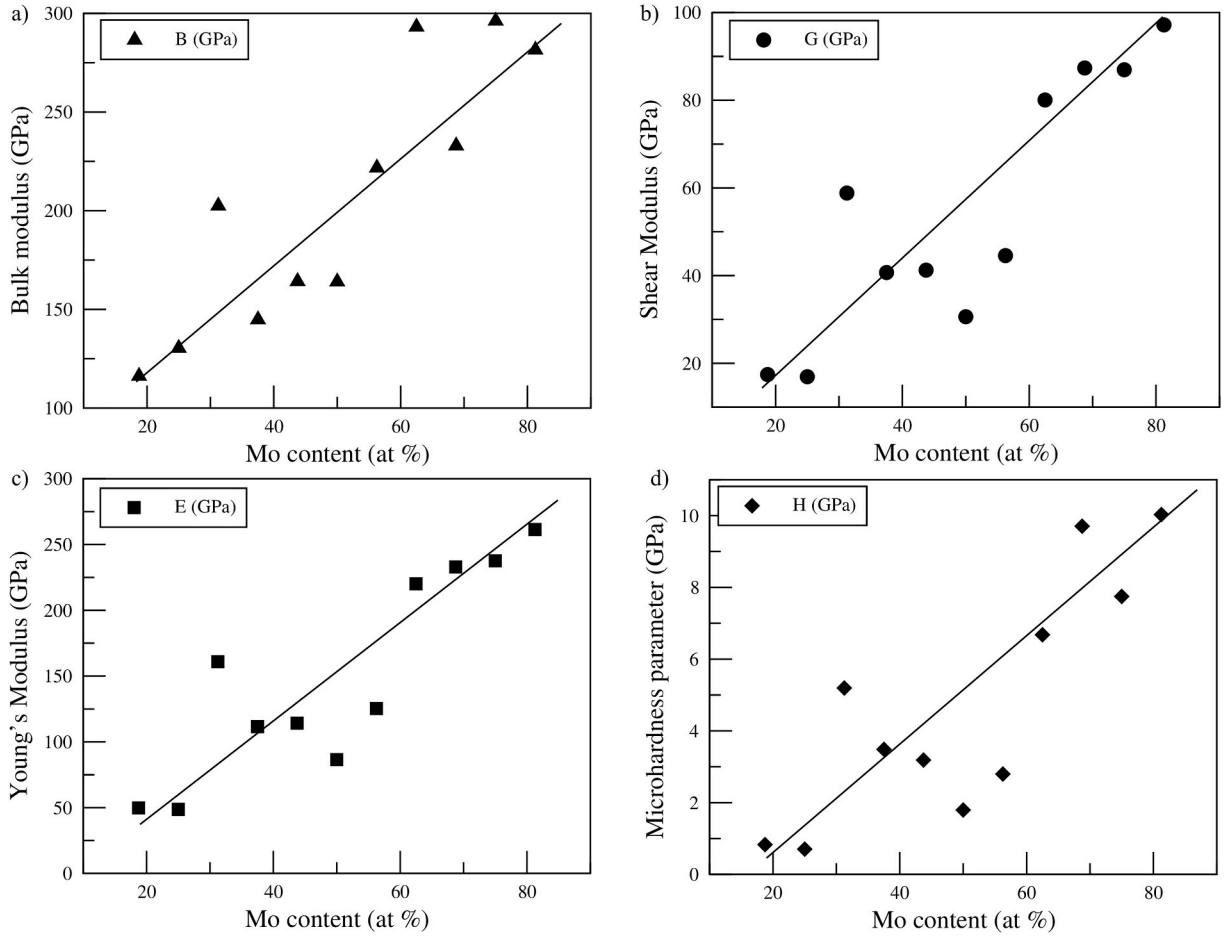

Fig. 4. The calculated a) bulk modulus $B(GPa)$, b) shear modulus $G(GPa)$, Young's modulus $E(GPa)$, microhardness $H(GPa)$ of the off-stoichiometric $Ti_{8-x}V_{4-y}Mo_{x+y+z}Al_{4-z}$ alloys and their shifting according to Mo content.

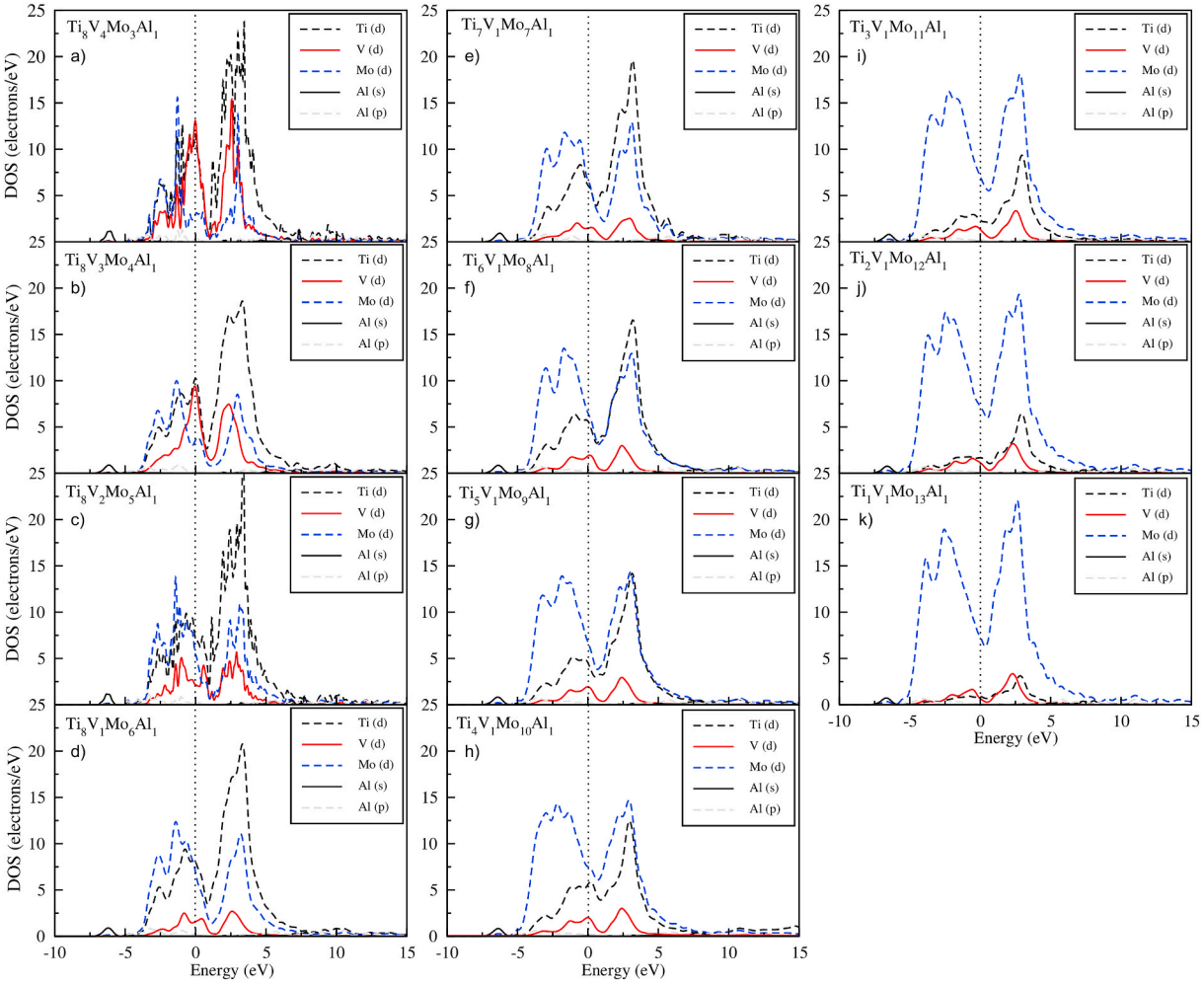

Fig. 5. The calculated partial density of states for off-stoichiometric crystal structures of $Ti_8V_4Mo_3Al_1$ (a), $Ti_8V_3Mo_4Al_1$ (b), $Ti_8V_2Mo_5Al_1$ (c), $Ti_8V_1Mo_6Al_1$ (d), $Ti_7V_1Mo_7Al_1$ (e), $Ti_6V_1Mo_8Al_1$ (f), $Ti_5V_1Mo_9Al_1$ (g), $Ti_4V_1Mo_{10}Al_1$ (h), $Ti_3V_1Mo_{11}Al_1$ (i), $Ti_2V_1Mo_{12}Al_1$ (j) and $Ti_1V_1Mo_{13}Al_1$ (k) alloys at zero pressure. The vertical dot line represents the Fermi level shifted to 0 eV. The main bonding peaks of $Ti_{8-x}V_{4-y}Mo_{x+y+z}Al_{4-z}$ alloys are originated from the contribution of valence electron numbers of Ti (3d), V (3d), Mo (4d) and Al 3s and Al (3p) orbits.

From a different point of view, to estimate the hardness of the studied phases of $Ti_{8-x}V_{4-y}Mo_{x+y+z}Al_{4-z}$ alloy, the microhardness parameter H was calculated using the formula given below [57]:

$$H = \frac{(1-2\upsilon)E}{6(1+\upsilon)} \tag{22}$$

As given in Fig. 4-a), The bulk modulus B value increases linearly in almost all phases due to increasing Mo concentration. However, a linear increase of bulk modulus B value in $Ti_8V_2Mo_5Al_1$, $Ti_4V_1Mo_{10}Al_1$, and $Ti_2V_1Mo_{12}Al_1$ phases is impaired. Focusing on Fig. 4-b), The shear modulus G showed a linear increase with increasing Mo concentration, but deviations from linearity were also observed in $Ti_8V_2Mo_5Al_1$, $Ti_6V_1Mo_8Al_1$, and $Ti_5V_1Mo_9Al_1$ phases. As shown in Fig. 4-c, the response of Young's modulus E and shear modulus G to increasing Mo concentration is very similar. Young's modulus E increases with increasing Mo concentration. As in the Shear modulus G, the linearity of the $Ti_8V_2Mo_5Al_1$, $Ti_6V_1Mo_8Al_1$, and $Ti_5V_1Mo_9Al_1$ phases deteriorate in Young's modulus E. Finally, it can be seen from Fig. 5-c) that the microhardness increases with increasing Mo concentration. Due to this behavior, the incompressibility of the off-stoichiometric $Ti_{8-x}V_{4-y}Mo_{x+y+z}Al_{4-z}$ alloys decreases.

3.3. Off-stoichiometric crystal electronic properties

To evaluate the electronic behavior of the off-stoichiometric $Ti_{8-x}V_{4-y}Mo_{x+y+z}Al_{4-z}$ alloys, the partial (PDOS) density of states was calculated, which describes the contributions from the individual electronic states, are shown in Fig. 5a)–k), respectively. The Fermi level is set to zero energy level and indicated by a vertical dashed line. Since there is no band gap around the Fermi level, all $Ti_{8-x}V_{4-y}Mo_{x+y+z}Al_{4-z}$ alloys exhibit a metallic character. All of the contributions from the valence electrons of the Ti (3*d*), V (3*d*), Mo (4*d*), and Al (3*s*,3*p*) atoms are in the range of −6.25 eV–15 eV.

In the phases where Mo concentration is 18.75% and 25.00%, the highest contribution to the near Fermi level originate mainly from Ti-3d (≅12.5 electrons/eV) and V-3d (≅ 12.5 electrons/eV) orbitals. The minimum contribution originates from Mo-4d (≅ 2.5 electrons/eV) orbitals. There is almost no contribution to this region from Al-s and Al-p orbitals for all phases. In the $Ti_8V_2Mo_5Al_1$ phase, where Mo concentration was 31.25%, Mo-4d and V-3d were displaced for the first time in the highest contributions near the Fermi level. While the highest contribution was in Ti-3d (≅ 10 electrons/eV) and Mo-4d (≅ 7.5 electrons/eV) orbitals, the lowest contribution was due to V-3d (≅ 2.5 electrons/eV). While the dominance of the Ti-3d and M-4d orbitals contributions around the Fermi level continues in the $Ti_8V_1Mo_6Al_1$, $Ti_7V_1Mo_7Al_1$, $Ti_6V_1Mo_8Al_1$, $Ti_5V_1Mo_9Al_1$, $Ti_3V_1Mo_{11}Al_1$, $Ti_2V_1Mo_{12}Al_1$ and

$Ti_1V_1Mo_{13}Al_1$ phases, it is seen that the minimum contributions are always caused by V-3d.

When we focus on the lower part of the Fermi level, due to the increase in Mo concentration, as shown in Fig. 5 from the $Ti_8V_4Mo_3Al_1$ phase to the $Ti_1V_1Mo_{13}Al_1$ phase direction the highest contribution originates from the Mo-4d (approximately 10–17.5 electrons/eV) orbitals. To this region, the contributions from Ti-3d is above V-3d below Mo-4d. However, in the $Ti_4V_1Mo_{10}Al_1$ phase, contributions from V-3d are suddenly more than Mo-4d.

To the upper part of the Fermi level, from the $Ti_8V_4Mo_3Al_1$ (18.75% Mo) phase to the $Ti_6V_1Mo_8Al_1$ (50% Mo) phase, the higher contributions emerge from the Ti-3d orbitals. Mo-4d and Ti-3d additives in the $Ti_5V_1Mo_9Al_1$ (56.25% Mo) phase are equal. As Mo concentration rises above 56.25%, the contributions from Mo-4d increase, while the contributions from Ti-3d decrease. In the above, the Fermi level, in all phases except the $Ti_4V_1Mo_{10}Al_1$ phase, contributions from Vi-3d orbitals are generally less than Ti-3d and Mo-4d.

The increase in Mo concentration decreases the peak heights of Ti atoms while increases the peak of Mo atoms. In particular, the height of the Ti-3d dominant peaks between 1 eV and 6 eV decreases severely as the Mo concentration increases. This behavior is seen in Fig. 5-f), g), h), i), j), k). In contrast, contributions from Mo-4d orbitals are carried from the upper part (0 eV–5 eV) to the lower part of the Fermi level. Especially, the contributions from the Mo-4d orbits in the range of −5 eV–0 eV (in the lower part of the Fermi level) dominate the contributions from the Ti, V, and Al atoms both in terms of peak height and energy width. However, the contributions from V-3d orbits at the fermi level decrease as the Mo concentration increases. However, since the contributions from V-3d are moved from the lower part Fermi level to the upper part Fermi level, the decrease in V concentration will adversely affect crystal stability. However, the tendency of electrons from Ti-3d and Mo-4d orbits to move to the lower part Fermi level is highly tolerant of instability caused by V atoms.

As shown in Fig. 5, there is strong hybridization between the Ti-3d and Mo-4d states in the range of −2.5 eV–2.5 eV at the lower and upper part Fermi levels. Further, The Ti- (3d) -Mo- (4d) bonds were moved to the lower energy region towards the lower part Fermi level. Therefore, the peak height and energy distribution width of the Ti- (3d) -Mo- (4d) bonds in this region increased. Accordingly, the effect of Ti- (3d) -Mo- (4d) bonds predominates over other orbitals. Ti-3d-Mo- (4d) bonds have been reported to have high binding energy in the study conducted by Li et al. [58]. Hence, the behaviors of Ti-3d-Mo- (4d) bonds and increased Mo concentration support the stability of the $Ti_{8-x}V_{4-y}Mo_{x+y+z}Al_{4-z}$ crystal structure. Also, as the Mo concentration increases, the peaks in the Fermi level decrease and broaden gradually towards the −2.5 eV and 2 eV regions. The width is greater in the lower part Fermi level in the dominant Mo-4d states. This is seen in Fig. 5-b), g), h), i), j) and k). This behavior may explain that the elastic modulus of the phases $Ti_8V_2Mo_5Al_1$, $Ti_5V_1Mo_9Al_1$, $Ti_4V_1Mo_{10}Al_1$, $Ti_3V_1Mo_{11}Al_1$, $Ti_2V_1Mo_{12}Al_1$, and $Ti_1V_1Mo_{13}Al_1$ have significantly higher values than the other phases. As a result, as Mo concentration increases in the $Ti_{8-x}V_{4-y}Mo_{x+y+z}Al_{4-z}$ alloys, both the Ti and V atoms which are toxic to human health are reduced (Al is fixed at the lowest rate) and more stable the off-stoichiometric $Ti_{8-x}V_{4-y}Mo_{x+y+z}Al_{4-z}$ crystal structures can be formed by the effect of Ti–Mo bonds.

4. Conclusion

In this study, the off-stoichiometric $Ti_{8-x}V_{4-y}Mo_{x+y+z}Al_{4-z}$ form of Ti–V–Al alloy, which is a good LWSMA candidate, is focused. To reduce toxic effects and increase biomaterial efficiency, the structural, mechanical, and electronic properties of the off-stoichiometric $Ti_{8-x}V_{4-y}Mo_{x+y+z}Al_{4-z}$ alloys have been studied systematically with Density Functional Theory (DFT) based ab-*initio* calculation methods.

- It was determined that as Mo concentration of the $Ti_{8-x}V_{4-y}Mo_{x+y+z}Al_{4-z}$ alloys increased, the formation and cohesive energies decreased. This behavior shows that thermodynamic and structural stability of the $Ti_{8-x}V_{4-y}Mo_{x+y+z}Al_{4-z}$ alloys increases due to the increase in Mo concentration.
- It has been found that all of the calculated elastic constants meet all the mechanical criteria given according to the crystal symmetries. However, due to the increasing Mo concentration, it was determined that there were phase transitions to the tetragonal, rhombohedral, and monoclinic crystal structures. But, it satisfies the mechanical criteria in the determined different phases. Therefore, all phases are mechanically stable.
- The bulk modulus B, shear modulus G, Young's modulus E, microhardness H, Poisson ratio υ, Pugh's ratio G/B of the off-stoichiometric $Ti_{8-x}V_{4-y}Mo_{x+y+z}Al_{4-z}$ have been calculated by using the Voigt-Reuss-Hill approximation. The results of G/B show that the ductility of all phases decreases with increasing Mo concentration. But, all phases have remained within the limits of ductility. Therefore, we studied all phases of material that have a ductile character. The plasticity of the $Ti_{8-x}V_{4-y}Mo_{x+y+z}Al_{4-z}$ alloys is downgraded with the increase of Mo concentration by the Poisson's ratio υ.
- The Young's modulus E of $Ti_8V_4Mo_3Al_1$ and $Ti_8V_3Mo_4Al_1$ phases were calculated as 49.84 GPa and 48.71 GPa, respectively. The human bone's Young's modulus E is in the range of 20–40 GPa. When our results are evaluated in terms of this criterion, $Ti_8V_4Mo_3Al_1$ and $Ti_8V_3Mo_4Al_1$ phases are very suitable candidates for real biomaterial applications. Also, with Young's modulus E of 86.5 GPa, the $Ti_6V_1Mo_8Al_1$ phase can be considered a good biomaterial candidate.
- The electronic structure shows that as Mo concentration increases the Ti-3d-Mo-4d bonds become stronger. Thus, the off-stoichiometric $Ti_{8-x}V_{4-y}Mo_{x+y+z}Al_{4-z}$ crystal structures become more stable by the effect of Ti–Mo bonds.

Credit author statement

Cengiz Soykan: Methodology, Software, Visualization, Writing - original draft, Reviewing and Editing.

Declaration of competing interest

The authors declare that they have no known competing financial interests or personal relationships that could have appeared to influence the work reported in this paper.

Acknowledgments

The author would like to thank the following institutions and agencies in carrying out this paper. Computations are carried out on TUBITAK-ULAKBIM clusters. This study is supported by the Department of Physics at Pamukkale University. The author would thank Dr. Şükrü YILDIZ to encourage to study Ti–V–Al alloys. The author would thank Dr. Murat ÇINARLI and Dr. Avni AKSOY for their contributions to study.

Appendix A. Supplementary data

Supplementary data to this article can be found online at https://doi.org/10.1016/j.physb.2020.412416.

References

[1] T. Maeshima, M. Nishida, Shape memory properties of biomedical Ti-Mo-Ag and Ti-Mo-Sn alloys, Mater. Trans. 45 (2004) 1096–1100, https://doi.org/10.2320/matertrans.45.1096.
[2] J.J. Gutiérrez-Moreno, Y. Guo, K. Georgarakis, A.R. Yavari, G.A. Evangelakis, Ch. E. Lekka, The role of Sn doping in theb-type Ti–25 at%Nb alloys: experimentand ab

initio calculations, J. Alloys Compd. 615 (2014) 676–679, https://doi.org/10.1016/j.jallcom.2014.05.024.
[3] Y.L. Zhou, D.M. Luo, Microstructures and mechanical properties of Ti–Mo alloys cold-rolled and heat treated, Mater. Char. 62 (2011) 931–937, https://doi.org/10.1016/j.matchar.2011.07.010.
[4] S.J. Dai, Y. Wang, F. Chen, Effects of annealing on the microstructures and mechanical properties of biomedical cold-rolled Ti–Nb–Zr–Mo–Sn alloy, Mater. Char. 104 (2015) 16–22, https://doi.org/10.1016/j.matchar.2015.04.004.
[5] P.S. Nnamchi, First principles studies on structural, elastic and electronic properties of new TiMoNbZr alloys for biomedical applications, Mater. Des. 108 (2016) 60–67, https://doi.org/10.1016/j.matdes.2016.06.066.
[6] Q. Chen, G.A. Thouas, Metallic implant biomaterials, Mater. Sci. Eng. R Rep. 87 (2015) 1–57, https://doi.org/10.1016/j.mser.2014.10.001.
[7] Y.H. Song, M.K. Kim, E.J. Park, H.J. Song, K.J. Anusavice, Y.J. Park, Cytotoxicity of alloying elements and experimental titanium alloys by WST-1 and agar overlay tests, Dent. Mater. 30 (2014) 977–983, https://doi.org/10.1016/j.dental.2014.05.012.
[8] A.V. Sandu, M.S. Baltatu, M. Nabialek, A. Savin, P. Vizureanu, Characterization and mechanical proprieties of new TiMo alloys used for medical applications, Materials 12 (2019) 2973, https://doi.org/10.3390/ma12182973.
[9] D.C. Ludwigson, Requirements for metallic surgical implants and prosthetic devices, Met. Eng. Quart. 5 (1965) 1–6.
[10] D.M. Bombac, M. Brojan, P. Fajfar, F. Kosel, R. Turk, Review of materials in medical applications, RMZ Mater. Geoenviron 54 (2007) 471–499.
[11] M.S. Baltatu, C.A. Tugui, M.C. Perju, M. Benchea, M.C. Spataru, A.V. Sandu, P. Vizureanu, Biocompatible titanium alloys used in medical applications, Rev. Chim. (Bucharest) 70 (2019) 1302–1306.
[12] S. Spriano, S. Yamaguchi, F. Bainoa, S. Ferraris, A critical review of multifunctional titanium surfaces:New frontiers for improving osseointegration and host response, avoiding bacteria contamination, Acta Biomater. 79 (2018) 1–22, https://doi.org/10.1016/j.actbio.2018.08.013.
[13] Z.G. Wang, Y. Li, W.J. Huang, X.L. Chen, H.R. He, Micro-abrasion-corrosion behaviour of a biomedical Ti-25Nb-3Mo-3Zr-2Sn alloy in simulated physiological fluid, J. Mech. Behav. Biomed. 63 (2016) 361–374, https://doi.org/10.1016/j.jmbbm.2016.07.010.
[14] R.W. Yi, H.Q. Liu, D.Q. Yi, W.F. Wan, B. Wang, Y. Jiang, Q. Yang, D.C. Wang, Q. Gao, Y.F. Xu, Q. Tang, Precipitation hardening and microstructure evolution of the Ti-7Nb-10Mo alloy during aging, Mater. Sci. Eng. C 63 (2016) 577–586, https://doi.org/10.1016/j.msec.2016.03.030.
[15] C. Chen, W. He, L. Ding, X. Song, J. Huang, T. Wang, G. Huang, First principles studies on the elastic, thermodynamic properties and electronic structure of $Ti_{15-x}Mo_xSn$ compounds, Curr. Appl. Phys. 18 (3) (2018) 280–288, https://doi.org/10.1016/j.cap.2017.12.008.
[16] P. Hohenberg, W. Kohn, Inhomogeneous electron gas, Phys. Rev. B 136 (1964) 864, https://doi.org/10.1103/PhysRev.136.B864.
[17] W. Kohn, L.J. Sham, Self-consistent equations including exchange and correlation effects, Phys. Rev. 140 (1965) 1133, https://doi.org/10.1103/PhysRev.140.A1133.
[18] W. Kohn, A.D. Becke, R.G. Parr, Density functional theory of electronic structure, J. Phys. Chem. 100 (1996) 974, https://doi.org/10.1021/jp960669l.
[19] G. Kresse, J. Furthmuller, Efficiency of ab-initio total energy calculations for metals and semiconductors using a plane-wave basis set, Comput. Mater. Sci. 6 (1996) 15–50, https://doi.org/10.1016/0927-0256(96)00008-0.
[20] G. Kresse, J. Furthmuller, Efficient iterative schemes for ab-initio total energy calculations using a plane-wave basis set, Phys. Rev. B 54 (1996) 11169, https://doi.org/10.1103/PhysRevB.54.11169.
[21] J. Hafner, Materials simulations using VASP a quantum perspective to materials science, Comput. Phys. Commun. 177 (2007) 6–13, https://doi.org/10.1016/j.cpc.2007.02.045.
[22] G. Kresse, J. Hafner, Ab initio molecular dynamics for liquid metals, Phys. Rev. B 47 (1993) 558, https://doi.org/10.1103/PhysRevB.47.558.
[23] G. Kresse, J. Hafner, Norm-conserving and ultrasoft pseudopotentials for first-row and transition elements, J. Phys. Condens. Matter 6 (1994) 8245, https://doi.org/10.1088/0953-8984/6/40/015.
[24] J.P. Perdew, K. Burke, M. Ernzerhof, Generalized gradient approximation made simple, Phys. Rev. Lett. 77 (1996) 3865, https://doi.org/10.1103/PhysRevLett.77.3865.
[25] M. Methfessel, A.T. Paxton, High-precision sampling for Brillouin-zone integration in metals, Phys. Rev. B 40 (1989) 3616–3621, https://doi.org/10.1103/PhysRevB.40.3616.
[26] H.J. Monkhorst, J.D. Pack, Special points for Brillouin-zone integrations, Phys. Rev. B 13 (1976) 5188–5192, https://doi.org/10.1103/PhysRevB.13.5188.
[27] V.M. Goldschmidt, Gesetze der Krystallochemie, Naturwissenschaften 14 (1926) 477–485, https://doi.org/10.1007/BF01507527.
[28] S.-H. Wei, L.G. Ferreira, James E. Bernard, A. Zunger, Electronic properties of random alloys: special quasirandom structures, Phys. Rev. B 42 (1990) 9622–9649, https://doi.org/10.1103/PhysRevB.42.9622.
[29] K.C. Hass, L.C. Davis, A. Zunger, Electronic structure of random Al0.5Ga0.5As alloys: test of the "special-quasirandom-structures'' description, Phys. Rev. B 42 (1990) 3757–3760, https://doi.org/10.1103/PhysRevB.42.3757.
[30] K. Otsuka, X. Ren, Physical metallurgy of Ti–Ni-based shape memory alloys, Prog. Mater. Sci. 50 (2005) 511–678, https://doi.org/10.1016/j.pmatsci.2004.10.001.
[31] T. Hara, T. Ohba, K. Otsuka, M. Nishida, Phase transformation and crystal structures of Ti2Ni3 precipitates in Ti–Ni alloys, Mater. Trans., JIM 38 (1997) 277–284, https://doi.org/10.2320/matertrans1989.38.277.
[32] M. Nishida, C.M. Wayman, R. Kainuma, T. Honma, Further electron microscopy studies of the $Ti_{11}Ni_{14}$ phase in an aged Ti-52at%Ni shape memory alloy, Scripta Metall. 20 (1986) 899–904, https://doi.org/10.1016/0036-9748(86)90463-1.
[33] T. Saburi, S. Nenno, T.J. Fukuda, Crystal structure and morphology of the metastable X phase in shape memory Ti-Ni alloys, J. Less Common Met. 125 (1986) 157, https://doi.org/10.1016/0022-5088(86)90090-1.
[34] T. Tadaki, Y. Nakata, K. Shimizu, K. Otsuka, Crystal structure, composition and morphology of a precipitate in an aged Ti-51 at.% Ni shape memory alloy, Trans. Jpn. Inst. Met. 27 (1986) 731–740, https://doi.org/10.2320/matertrans1960.27.731.
[35] L.F. Zhu, M. Friák, A. Dick, B. Grabowski, T. Hickel, F. Liot, D. Holec, A. Schlieter, U. Kühn, J. Eckert, Z. Ebrahimi, H. Emmerich, J. Neugebauer, First-principles study of the thermodynamic and elastic properties of eutectic Fe–Ti alloys, Acta Mater. 60 (2012) 1594–1602, https://doi.org/10.1016/j.actamat.2011.11.046.
[36] R. Karre, M.K. Niranjan, S.R. Dey, First principles theoretical investigations of low young's modulus beta Ti-Nb and Ti-Nb-Zr alloys compositions for biomedical applications, Mater. Sci. Eng. C 50 (2015) 52–58, https://doi.org/10.1016/j.msec.2015.01.061.
[37] F. Mouhat, F.X. Coudert, Necessary and sufficient elastic stability conditions in various crystal systems, Phys. Rev. B 90 (2014), 224104, https://doi.org/10.1103/PhysRevB.90.224104.
[38] Y. Le Page, P. Saxe, Symmetry-general least-squares extraction of elastic data for strained materials from ab initio calculations of stress, Phys. Rev. B 65 (2002) (2002), 104104, https://doi.org/10.1103/PhysRevB.65.104104.
[39] J.J. Wang, F.Y. Meng, X.Q. Ma, M.X. Xu, L.Q. Chen, Lattice, elastic, polarization, and electrostrictive properties of $BaTiO_3$ from first principles, J. Appl. Phys. 108 (2010), 034107, https://doi.org/10.1063/1.3462441.
[40] S. Piskunov, E. Heifets, R.I. Eglitis, G. Borstel, Bulk properties and electronic structure of $SrTiO_3$, $BaTiO_3$, $PbTiO_3$ perovskites: an ab initio HF/DFT study, Comput. Mater. Sci. 29 (2004) 165–178, https://doi.org/10.1016/j.commatsci.2003.08.036.
[41] R. Khenata, M. Sahnoun, H. Baltache, M. Rerat, A.H. Rashek, N. Illes, B. Bouhafs, First-principle calculations of structural, electronic and optical properties of $BaTiO_3$ and $BaZrO_3$ under hydrostatic pressure, Solid State Commun. 136 (2005) 120–125, https://doi.org/10.1016/j.ssc.2005.04.004.
[42] G. Vaitheeswaran, V. Kanchana, S. Heathman, M. Idiri, T. Le Bihan, A. Svane, A. Delin, B. Johansson, Elastic constants and high-pressure structural transitions in lanthanum monochalcogenides from experiment and theory, Phys. Rev. 75 (2007), 184108, https://doi.org/10.1103/PhysRevB.75.184108.
[43] Z. Charifi, H. Baaziz, Y. Saeed, Ali Hussain Reshak, F. Soltani, The effect of chalcogen atom on the structural, elastic, and high-pressure properties of XY compounds (X = La, Ce, Eu, and Y = S, Se, and Te): an ab initio study, Phys. Status Solidi B 249 (2012) 18, https://doi.org/10.1002/pssb.201147216.
[44] A. Bouhemadou, R. Khenata, M. Maamache, Structural phase stability and elastic properties of lanthanum monochalcogenides at high pressure, J. Mol. Struct. Theochem. 777 (2006) 5–10, https://doi.org/10.1016/j.theochem.2006.08.031.
[45] X. Li, J. Zhao, J. Xu, Mechanical properties of bcc Fe-Cr alloys by first-principles simulations, Front. Physiol. 7 (2012) 360–365, https://doi.org/10.1007/s11467-011-0193-0.
[46] W. Voigt, Lehrbuch der Kristallphysik, Leipzig, Taubner, 1928, https://doi.org/10.1007/978-3-663-15884-4.
[47] A. Reuss, Berechnung der Fließgrenze von Mischkristallen auf Grund der Plastizitätsbedingung für Einkristalle, Z. Angew. Math. Mech. 9 (1929) 55–66, https://doi.org/10.1002/zamm.19290090104.
[48] R. Hill, The elastic behaviour of a crystalline aggregate, Proc. Soc. London A 65 (5) (1952) 349–354, https://doi.org/10.1088/0370-1298/65/5/307.
[49] Q. Liu, Z. Liu, L. Feng, Calculations of structural, elastic, electronic, and optical properties of trigonal CdI_2, Phys. Status Solidi B 248 7 (2011) 1629–1633, https://doi.org/10.1002/pssb.201046481.
[50] J.P. Watt, Hashin-Shtrikman bounds on the effective elastic moduli of polycrystals with monoclinic symmetry, J. Appl. Phys. 51 (1980) 1520, https://doi.org/10.1063/1.327803.
[51] Z.J. Wu, E.J. Zhao, H.P. Xiang, et al., Crystal structures and elastic properties of super hard IrN2 and IrN3 from first principles, J. Phys. Rev. B. 76 (5) (2007), 054115, https://doi.org/10.1103/PhysRevB.76.054115.
[52] U.K. Chowdhury, M.A. Rahman, M.A. Rahman, M. Bhuiyan, M.L. Ali, Ab initio study on structural, elastic, electronic and optical properties of cuprate based superconductor, Cogent Phys. 3 (2016), 1231361, https://doi.org/10.1080/23311940.2016.1231361.
[53] K. Benkaddour, A. Chahed, A. Amar, H. Rozale, A. Lakdja, O. Benhelal, A. Sayede, First-principles study of structural, elastic, thermodynamic, electronic and magnetic properties for the quaternary Heusler alloys CoRuFeZ (Z = Si, Ge, Sn), J. Alloys Compd. 687 (2016) 211–220, https://doi.org/10.1016/j.jallcom.2016.06.104.
[54] M.A. Rahman, M.Z. Rahaman, M.A. Rahman, The structural, elastic, electronic and optical properties of MgCu under pressure: a first-principles study, Int. J. Mod. Phys. B 30 (2016), 1650199, https://doi.org/10.1142/S021797921650199X.
[55] S. Pugh, XCII. Relations between the elastic moduli and the plastic properties of polycrystalline pure metals, London Edinburgh Philos. Mag. J. Sci. London, Edinburgh Dublin Philos. Mag. J. Sci. 45 (1954) 823–843, https://doi.org/10.1080/14786440808520496.
[56] M.A. Rahman, M.Z. Rahaman, M.A.R. Sarker, First principles investigation of structural, elastic, electronic and optical properties of $HgGeB_2$ (BP, As)

chalcopyrite semiconductors, Comput. Condens. Matter 9 (2016) 19–26, https://doi.org/10.1016/j.cocom.2016.09.001.

[57] E.S. Yousef, A. El-Adawy, N. El-KheshKhany, Effect of rare earth (Pr_2O_3, Nd_2O_3, Sm_2O_3, Eu_2O_3, Gd_2O_3 and Er_2O_3) on the acoustic properties of glass belonging to bismuth–borate system, Solid State Commun. 139 (2006) 108–113, https://doi.org/10.1016/j.ssc.2006.05.022.

[58] H. Li, Z.J. Wang, G.D. Sun, P.F. Yu, W.X. Zhang, First-principles study on the structural, elastic and electronic properties of Ti2SiN under high pressure, Solid State Commun. 237–238 (2016) 24–27, https://doi.org/10.1016/j.ssc.2016.03.019.